

Synchrotron X-ray Fluorescence Analysis of Copper and Zinc in Silicate and Oxide Minerals from Granitoid Rocks

Daniel P. Core^{1,2}, Stephen E. Kesler¹, Eric J. Essene¹, Eric B. Dufresne³, Roy Clarke³, Dohn A. Arms⁴, Don Walko⁴, and Mark L. Rivers⁵

¹Department of Geological Sciences
University of Michigan
Ann Arbor, MI 48109-1063

²Geoinformatics
PO Box 1675
West Perth WA 6872, Australia

³Department of Physics
University of Michigan
Ann Arbor, MI 48109-1063

⁴Argonne National Laboratories
MHATT-CAT
Argonne, IL 60439

⁵The University of Chicago
c/o Argonne National Laboratory
9700 S. Cass Avenue, Bldg. 434/A004
Argonne, IL 60439

Abstract

Synchrotron X-ray fluorescence (SXRF) analyses for Cu, Zn and Fe were carried out on magmatic minerals from intrusive and volcanic rocks in the Bingham-Park City Belt, Utah. The main goal of the study was to determine background Cu and Zn contents of magmatic minerals, and search for zoning patterns that might record separation of a magmatic vapor phase containing Cu and Zn. The combination of low detection limits and small analytical footprint makes SXRF the preferred method for tests of this type. Results of the study show that the distribution of Zn in magmatic minerals mimics that of Fe whereas Cu does not and, instead, is enriched in patches that probably reflect the presence of submicroscopic phases. At least some

of the inclusions include chlorite or related alteration minerals. Copper concentrations are about 10 ppm in unaltered mafic silicate minerals and 20 ppm in magnetite, confirming that Cu behaves incompatibly during crystallization. Zinc concentrations range from 500 to 1000 ppm in unaltered magnetite and mafic silicate minerals, confirming that Zn behaves compatibly. Phase equilibria suggest that the substitution of trace levels of Zn and Cu in silicates and oxides forms at lower fO_2 and fS_2 than the equivalent assemblage involving Cu- and Zn-sulfides. Decreasing Cu concentrations from core to rim were observed in biotite from the Keetley volcanic rocks, but were absent in intrusive rocks. Cu-rich rims on biotite from the intrusive rocks probably reflect post-crystallization mobility of Cu, possibly recording the late migration of a magmatic vapor phase. Introduction

Granitoid magmas are associated with a wide range of magmatic-hydrothermal ore deposits containing Cu and Zn, and are thought to be the main source of these metals (Candela, 1989; Burnham, 1997). Along with many other trace elements, Cu and Zn form complex ions that partition strongly into a magmatic vapor phase, from which they are deposited by cooling and reaction with surrounding rock and fluids. Although many chemical and physical factors affect whether an intrusion can form an ore deposit, one of the most important is the availability of metals when the magmatic vapor phase forms. If metals behave compatibly and partition into condensed phases in the melt, they will be depleted in the residual magma, making it less likely to form an ore deposit.

Surprisingly little direct information is available on whether transition metal elements behave compatibly or incompatibly during crystallization of magmas. Some granitoid rocks contain primary sulfide minerals, but they are scarce and have not been shown to have a systematic distribution with respect to crystallization of magmatic silicate and oxide minerals (Banks, 1974, 1982; Borrok et al., 1999). Magmatic silicate and oxide minerals have very low and poorly known transition metal element contents that might retain information on the geochemical evolution of metals in their host magmas. Early studies of magmatic minerals based on analysis of mineral separates showed that (1) Cu and Zn appear to partition into magmatic oxides and mafic silicates, (2) Cu contents of these minerals vary much more than Zn contents, (3) high Cu contents are associated with Cu mineralization in some areas, and (4) biotite containing chlorite or other alteration phases has higher Cu contents (Parry and Nackowski, 1963; Al-Hashimi and Browlow, 1970; Lovering et al., 1970; Blaxland, 1971; Brabec and White, 1971; Graybeal, 1973; Banks, 1974; Kesler et al., 1975; Rehrig and McKinney, 1976). Electron microprobe studies of mafic silicate and oxide minerals confirmed these conclusions, but they were not able to provide significant additional information on metal zoning patterns because of the high detection limits for Cu and Zn (Banks, 1974; Willson, 1979). Ion probe (SIMS) analyses, which had the advantage of significantly lower detection limits, showed

that unaltered mafic silicate minerals contain 2 to 20 ppm Cu, whereas oxide minerals contain up to 200 ppm (Banks, 1982; Hendry et al., 1982, 1985). Using PIXE methods, Ewart and Griffin (1994) reported generally similar Cu and Zn contents of mafic silicate minerals, and Stimac and Hickmott (1994) reported that Zn is partitioned into ilmenite and pyroxene. However, the relatively large analytical footprint of these methods also limited the amount of data that could be obtained on zoning patterns for these elements.

In this study, Zn and Cu were measured in silicate and oxide minerals using synchrotron X-ray fluorescence (SXRF). SXRF analysis is the best tool for studies of this type because it combines very low detection limits with a small analytical footprint, thus allowing detection of zoning patterns in individual mineral phases. Work focused on igneous rocks in the Bingham-Park City belt in Utah, which contains the world-class Bingham porphyry copper deposit. Preliminary results suggest that Cu and Zn behave very differently during magmatic crystallization and that both elements are redistributed in otherwise fresh igneous rocks by late hydrothermal fluids.

Crystal Chemistry of Cu and Zn

The crystal chemistry of Zn and Cu in ordinary minerals provides insights about their geochemical behavior. Both Zn and Cu are ordinarily chalcophile elements and form sulfide minerals, or in some cases, a separate sulfide liquid when sulfide is available in a magma. At high fO_2/fS_2 , however, sulfate is stable over sulfide species and most sulfides are not stable (Holland, 1959, 1965). Then ferromagnesian silicates and oxides may be able to sequester these elements into their structures, at least at the 10-100 ppm level. Zinc is generally compatible in ferromagnesian silicates and oxides, such that it partitions into the crystalline solid over a coexisting silicate liquid. The ionic radius of Zn^{2+} , Cu^{1+} and Cu^{2+} ions in octahedral sites is on the order of 0.9 Å, still able to fit into those sites but large enough to fit less easily (Shannon, 1976).

Copper tends to form covalent bonds in silicates and usually occurs in the 1+ valence at fO_2 below the hematite-magnetite buffer. It is excluded from most ferromagnesian silicates, although tourmaline may have high Cu (Jiang et al., 2000), where it substitutes for Al in the Y site (MacDonald and Hawthorne, 1995). At more oxidizing conditions, Cu may assume 2+ valence, and with its Jahn-Teller behavior, prefers unusual structures with a square planar site such as diopside, or those with distorted V or VI sites. However, both Cu and Zn may partition into spinel structures such as magnetite, where Zn generally prefers the IV over the VI site, and Cu^{2+} enters the VI site as cuprospinel ($CuFe_2O_4$) solid solution (Burns, 1993). Experimental studies in magnetite show that Cu substitutes as Cu^{1+} at low levels, whereas at high levels it enters as Cu^{2+} (Sapozhnikova et al., 1981).

Zinc readily substitutes into Fe-bearing silicate minerals if it is not sulfidized to form sphalerite. Examples of such substitutions include petedunnite ($\text{CaZnSi}_2\text{O}_6$) solid solution in clinopyroxene, $\text{CaZnSi}_3\text{O}_8$ solid solution in plagioclase, franklinite (ZnFe_2O_4) in magnetite, and hendricksonite ($\text{KZn}_3\text{Si}_3\text{AlO}_{10}(\text{OH})_2$) solid solution in biotite. Zinc can also be found at varying levels in magmatic sulfides. Rarely magmatic sphalerite is reported as inclusions, for instance in phenocrysts from granitoids and rhyolites from the Bingham-Park City area (Borrok et al., 1999). Zinc also substitutes at low levels into ISS and pyrrhotite during crystallization of igneous rocks. Ewart and Griffin (1994) showed that Zn has a partition coefficient higher than one for most silicate and oxide phases. It strongly partitions into magnetite with a coefficient as high as 70.

Geologic Setting of Samples Used in the Study

The Bingham-Park City belt (BPCB) consists of 15 granitoid intrusions and coeval dike and volcanic rocks, which crop out in an E-W trending belt in central Utah that extends from the Oquirrh Mountains on the west through the Wasatch Range on the east (Figure 1). Samples were obtained from the Soldiers Canyon and Last Chance stocks (from west to east) in the Oquirrh Mountains, and the Alta, Clayton Peak, Ontario, and Pine Creek stocks (from west to east) in the Wasatch Range, as well as from the Ohio Copper dike in the Bingham district and the Keetley volcanic rocks in the Wasatch Range. The BPCB magmas probably formed by partial melting of lower crustal equivalents of the amphibolites in the Little Willow Formation and were emplaced in an extensional tectonic regime (Vogel et al., 2001). Emplacement depths of intrusions in the Wasatch Range varied from about 12 km on the west to about 1 km on the east and were similarly shallow in the Oquirrh Range (John, 1989).

The intrusive system at Bingham is associated with the Bingham porphyry copper deposit (PCD), the largest in North America (Phillips et al., 1997). Intrusive rocks of the BPCB were emplaced between 39.8 Ma and 30.5 Ma, and igneous activity in the Bingham district took place near the start of this period between 39.8 and 37.6 Ma (Warnaars et al., 1978; Deino and Keith, 1997; Vogel et al., 2001). Earliest intrusive phases at Bingham, including the pre-ore Last Chance and Bingham stocks and Phoenix dike, have a U-Pb zircon age of 38.6 ± 0.2 Ma (Parry et al., 2001). These were followed by the syn-mineralization quartz monzonite porphyry (QMP), which contains zircons with an age of 37.3 ± 0.3 Ma and hydrothermal biotite with an $^{40}\text{Ar}/^{39}\text{Ar}$ age of 37.6 ± 0.1 Ma (Parry et al., 2001; Core, 2004). Three later porphyries formed minor Cu mineralization, and all intrusive phases are cut by the Ohio Copper post-mineral dike. Molybdenum mineralization, which post-dates emplacement of all exposed intrusive rocks, has a Re-Os age of 37.0 ± 0.3 Ma, indicating a very short time period for mineralization at Bingham (Chesley and Ruiz, 1997; Redmond, 2002). Small, uneconomic porphyry copper deposits are also associated with the Soldiers Canyon stock in the Oquirrh Range and the Alta and Park

Premier stocks in the Wasatch Range (John, 1989). K-Ar and Ar-Ar ages for the Park Premier deposit suggest that it was roughly coeval with its host stock (John et al., 1997).

Analytical Methods

Synchrotron X-ray Fluorescence

Minerals were analyzed by synchrotron X-ray fluorescence (SXRF) using a sector seven beam-line (MHATT-CAT) at the Advanced Photon Source at Argonne National Labs. The relatively low detection limit of the SXRF method, especially when combined with its small analytical footprint, allowed analysis of Cu and Zn contents for all silicate minerals, including those with very low levels. This contrasts with most previous SIMS and other micro-analytical studies, which have focused on analysis of oxide and mafic silicate minerals, in part because their higher contents of Cu and Zn made them easier to analyze.

Analyses were made on grains in thin sections mounted on Suprasil pure silica glass to avoid contamination from high background concentrations that would be present in normal glass slides. In order to minimize the volume sampled during analyses, thin sections were ground to a thickness of 10 μm . The samples were examined optically and unaltered grains with clear paragenesis were selected for analysis. SXRF analyses were made using an X-ray beam with incident energy of 14 kV. The beam was focused to a spot size of approximately 4 μm using Pd coated mirrors in a Kirkpatrick-Baez (KB) orientation (Kirkpatrick and Baez, 1948). The beam was focused on a Nd-YAG crystal and the light from the fluorescence of the YAG was reflected to a camera. The size of the beam was minimized by adjusting the KB mirrors and monitored by moving a tungsten wire into the path of the beam and monitoring the flux with an ion chamber located behind the wire.

Samples were viewed through a microscope objective with a long working distance, which was attached to a closed-circuit video system. The beam caused visible fluorescence allowing determination of its approximate location on the sample. In a few samples a map of the Fe content in the area of interest was used to provide additional information about the location of spot analyses. This map permitted location of the beam within 5 μm .

Data were collected using a single element Ge detector placed 8 cm from the sample. A 100 μm high-purity aluminum filter was placed in front of the detector to prevent it from being flooded by the high X-ray flux. Peak intensities were corrected for absorption by the Al filter. Spectra were collected for 120 s and background subtraction was done using MCApro (Smith and Rivers, 1995). Concentrations of Cu and Zn were determined using Fe as an internal standard. Ratios of Cu to Fe were calculated using the method of Criss (1977). Detection limits for Cu were between 0.1-0.5 ppm for silicates and 5-10 ppm for oxides depending on the Fe content of the mineral. Precision of these analyses is generally less than 2% two-sigma. Accuracy is not this high due to errors introduced from using an internal standard, but it should

be less than 10% two-sigma. In addition to point analyses, traverses and maps were made on some of the grains. Step sizes of 2 and 5 μm were used for traverses and maps, respectively. The $K\alpha$ peaks of the elements were monitored for 1-2 seconds on each step.

Electron Microprobe

The major element composition of all spots that were analyzed by SXRF was also measured by electron microprobe analysis (EMPA) using a Cameca SX100 electron microprobe at the University of Michigan. All minerals were analyzed for Fe, Ca, Na, Al, Si, Ti, Ba, Mg, Mn, and K at 15 kV operating voltage and 10 nA sample current. A focused beam was rastered on a 5 μm spot to minimize beam damage and element migration and to mimic the size of the SXRF beam (although the EMPA beam did not penetrate to the same depth as the SXRF beam). Natural and synthetic oxide and silicate minerals were used as standards. Counting times were 20 s for all elements except Fe, which was analyzed for 40 s.

Analytical Results

Average Abundances of Cu and Zn

Magnetite has the highest average Cu content (210 ppm) of any magmatic mineral. Magmatic silicate minerals, listed in order of declining Cu content, average 120 ppm for biotite, 40 ppm for hornblende, 28 ppm for pyroxene, 22 ppm for ilmenite and 5 ppm for feldspar. Average Zn contents are highest in magnetite (2400 ppm), and averages for magmatic silicate minerals, listed in declining order, are biotite (790 ppm), ilmenite (550 ppm), hornblende (480 ppm), pyroxene (370 ppm), and lowest in feldspar (14 ppm).

Chlorite grains in most samples were too small to analyze, with the exception of two samples of the Alta stock containing large grains of biotite that had been altered to chlorite. The Cu contents of these grains are between 29 and 570 ppm, higher than the unaltered parts of adjacent biotite grains, which contain less than 10 ppm Cu. There is a dramatic difference between the two samples analyzed: chlorite from sample A20-12 has an average Cu content of 400 ppm and that from sample A19-18 has an average Cu content of 28 ppm. Chlorite from both samples have similar Zn contents of 1200 to 1500 ppm. On the basis of this very limited sampling, chlorite has average Cu and Zn concentrations of 250 and 1270 ppm, respectively, making it the most important mineral hosting Cu and the second most important for Zn.

Cu-rich Zones

Average trace element abundances of Cu and Zn are somewhat misleading, especially for Cu, because they exhibit strongly skewed distributions in most minerals. The Cu levels are bimodal, even though they are plotted on a geometric scale, whereas Zn is largely unimodal with some anomalous high values even when plotted on an arithmetic scale (Figure 2). This difference in Cu and Zn is clearly seen in Figure 3, an X-ray map of a biotite grain from the Clayton Peak stock (CP13-14), where Zn and Fe show similar smooth variations in

concentration within the biotite and Cu is strongly enriched in patches and along the rims of grains. Similar 10 to 50 μm Cu-rich patches are present in most other minerals that were analyzed, including magnetite and feldspars, although they are least common in the Keetley volcanic rocks. In view of the patchy distribution of Cu in these minerals, Cu analyses were divided into those from patches of this type (Cu-rich) and those from the surrounding, Cu-poor mineral. High Cu zones were found by making traverses across the grains and locating the areas with anomalous Cu values. Since the grains had variable background values of Cu, the Cu content required to be classified as high Cu also varied. This led to slight overlap of the high and low Cu zones for the different minerals. Most high-Cu analyses do not have anomalous Zn contents, however (Figure 2).

The Cu-enriched zones are probably inclusions of a Cu-rich mineral or fluid inclusion. Inclusions that might account for the high-Cu zones were not seen in most thin sections, although the presence of submicroscopic inclusions cannot be ruled out. No sulfide is visible in the patches; Fe concentrations do not appear to reflect the presence of sulfide, but S could not be analyzed at the same time as Cu, Zn, and Fe during the SXRF analyses. Banks (1974, 1982) concluded that Cu enrichment in mafic minerals, especially biotite, was due to the formation of chlorite or related alteration minerals. Ilton and Veblen (1988, 1993) showed that weathered biotite has expanded layers that contain native Cu that is thought to have formed during oxidation of nearby sulfides. Samples in this study did not undergo extensive weathering, but do show local propylitic alteration, suggesting that chloritization could be the cause of at least some Cu enrichment. Support for this interpretation is seen in the Cu-rich chlorite-bearing rim consisting of chlorite, sphene, magnetite, and K-feldspar that surrounds a biotite rim (Figure 4).

Another type of inclusion might account for some of the Cu patches, however. Samples in which the mafic minerals were classified as altered (usually with visible chlorite in thin section) have higher Cu contents, on average, than do samples with no visible alteration (Figure 5). Note in the biotite plot (Figure 5A), that only some of the altered samples are enriched in Zn, whereas all of them are enriched in Cu. Furthermore, analyses for chlorite in the Alta stock plot between the main field of biotite analyses and the three samples with highly anomalous Cu and Zn. We do not have enough analyses of chlorite to be sure, but the available data suggest that chlorite inclusions are enriched in both Cu and Zn. The identity of the Cu-rich patches is unclear, although they could be sulfide minerals. For instance, magnetite and feldspar are not as likely to contain inclusions of chlorite. Li et al. (1998) found with TEM studies that partially chloritized biotite contained Cu sulfides, which they suggested formed by metasomatism during hydrothermal activity rather than by isochemical oxidation/reduction reactions.

Magmatic Cu and Zn Substitution Levels in Silicates and Oxides

Regardless of their origin, the Cu-rich patches and rims are probably not good indicators of the original magmatic Cu content of these minerals, and better information can be obtained from the samples that form the low-Cu population in Figure 3. For instance, unaltered biotite contains 0.6 to 74 ppm Cu, with a median value of 8 ppm, whereas high-Cu zones contain 20 to more than 1000 ppm Cu. The Cu contents of unaltered biotite are highest in the Soldier Canyon and Clayton Peak stocks. Zinc contents range from 468 to 958 ppm, with a median value of 728 ppm. The Pine Creek stock has the highest concentration of Zn in biotite, ranging from 683 to 958 ppm.

Clinopyroxene grains from the Clayton Peak, Last Chance, and Soldier Canyon stocks contain 2 to 20 ppm Cu with a median value of 6 ppm, whereas enriched zones contain 26 to 120 ppm Cu. Clinopyroxene from the Last Chance stock, which is in part of the magmatic succession that led to the Bingham porphyry Cu deposit, has the lowest Cu content of the group, ranging from 2 to 6 ppm with one value at 15 ppm. Concentrations of Zn in clinopyroxene range from 200 to 610 ppm with a median value of 350 ppm and are similar for all intrusions.

Hornblende samples can be divided into two groups, a low-Cu group containing 2 to 60 ppm Cu and a high-Cu group with 40 to 200 ppm Cu. Overlap in the two groups results from high-Cu patches being surrounded by biotite with very low Cu contents. The low-Cu group includes hornblendes from the Alta, Clayton Peak, Pine Creek and Last Chance stocks and the Keetley volcanic rocks. The high-Cu group comes largely from the Keetley volcanic rocks with one sample each from the Clayton Peak and Ontario stocks. Zinc concentrations in hornblende range from 220 to 700 ppm with a median of 510 ppm, and are highest in the Pine Creek stock.

Even after excluding the high-Cu patches, magnetite has the highest Cu concentration of any mineral analyzed ranging from 6 to 100 ppm, with a median of 22 ppm. High Cu zones within magnetite grains contain 50 to 1900 ppm Cu. The concentration of Zn in magnetite is the highest of any mineral, with a range of 90 to 7800 ppm and median of 1600 ppm. Magnetite from the Alta stock contains much less Zn than other stocks. Ilmenite from the Last Chance stock contains 5 to 50 ppm Cu with a median value of 21 ppm. Zinc in ilmenite ranges from 310 to 1100 ppm with median of 470 ppm.

The Cu and Zn contents of feldspars are less than those for mafic silicate and oxide minerals. The Cu ranges from 1 to 11 ppm with a median of 4 ppm, although there were a few high Cu zones in feldspars with 20 to 460 ppm. Concentration of Zn ranges from 2 to 28 ppm with a median of 16 ppm.

Correlations and Zoning of Cu, Zn and Fe

Figure 6 shows relations among Cu, Zn and Fe abundances in the main minerals analyzed in this study. Analyses are divided into high-Cu and low-Cu categories. The different distributions shown by Cu and Zn makes it unlikely that they are strongly correlated (Fig. 3).

This interpretation is supported by the plots in Figure 6, where Cu-Zn relations are entirely random for biotite, hornblende and pyroxene. The Cu and Zn are positively correlated for magnetite, however, especially the high-Cu analyses, and for the feldspars, whereas they are random for biotite, hornblende, and pyroxene. The weak negative correlation seen in the magnetite data simply reflects the high Ti content of magnetite in the high-Cu samples, and a somewhat better Cu-Fe correlation is seen in the feldspars. The correlations of Zn vs. Fe are somewhat better for all minerals with the possible exception of magnetite, and they are strong for feldspar.

Discussion

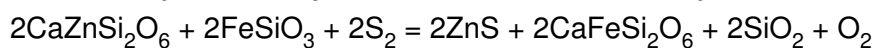
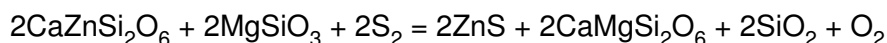
Sulfidation Reactions for Cu and Zn

Substitution of Cu and Zn into silicate and oxide minerals is buffered by one or more reactions forming sulfide-bearing assemblages that depend on oxygen and sulfur fugacities.

Petedunnite substitution in clinopyroxene is buffered by:

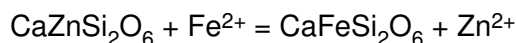


(Essene and Peacor, 1987). In the absence of wollastonite and in the presence of hypersthene and augite it would be buffered by:



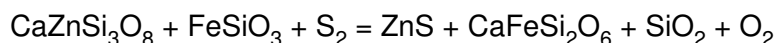
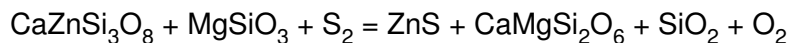
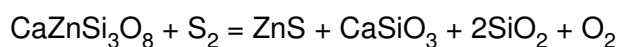
Two pyroxene assemblages occur in some of the granitoids under study (Core, 2004).

Thermodynamic and mixing data for petedunnite in clinopyroxene could be derived using in part the experimental data (Rothkopf and Fehr, 1998) to allow calibration of these reactions in $f\text{S}_2$ - $f\text{O}_2$ space at a fixed P-T. However, in the absence of sphalerite they provide only a limit to oxygen and sulfur fugacities. Ionic equilibria could also be considered in the presence of a vapor phase:

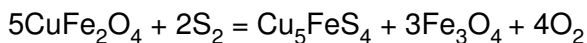


The composition of the pyroxene could be contoured on a diagram of $\log(a\text{Zn}^{2+})/\log(a\text{Fe}^{2+})$ vs. T at a fixed P. If the activity of Fe^{2+} in the parent magma can be estimated, the amount of Zn^{2+} that should also be present could also be estimated.

Substitution of Zn in feldspar may be understood relative to the synthetic phase $\text{CaZnSi}_3\text{O}_8$, which is a feldspar structure. Derivation of its thermodynamic properties from the experiments of Fehr and Huber (2001) and application of a selected thermodynamic model would allow calculation of reactions based on:



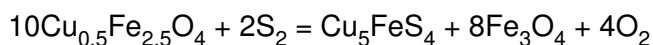
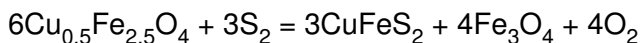
The latter two reactions would apply in the presence of the assemblage plagioclase-clinopyroxene-orthopyroxene-quartz-sphalerite. Franklinite and cuprospinel substitutions in magnetite are buffered by reactions such as the following:



Sphalerite buffers franklinite substitution in magnetite, and chalcopyrite or bornite buffer cuprospinel in magnetite.

Bornite is a magmatic mineral in some oxidized granitoids, and the Cu content of magnetite in equilibrium with bornite will constrain oxygen and sulfur fugacities if a mixing model for cuprospinel-magnetite is available. Some experimental data in the system $\text{CuFe}_2\text{O}_4\text{-Fe}_3\text{O}_4$ (Katkov and Lykasov, 2003) provide information on the mixing properties for this binary. However, at minor levels, Cu substitutes in magnetite via $\text{Cu}^{1+}\text{Fe}^{3+} = 2\text{Fe}^{2+}$, as shown by experiments on the system $\text{CuFe}_2\text{O}_4\text{-Cu}_{0.5}\text{Fe}_{2.5}\text{O}_4\text{-Fe}_3\text{O}_4$ (Sapozhnikova et al., 1981).

Alternative reactions would then apply:

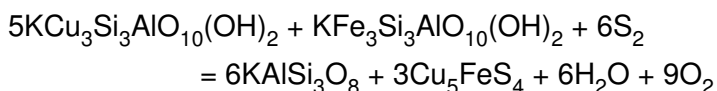


The slopes and positions of the last four reactions in $f\text{S}_2\text{-}f\text{O}_2$ space thus depend on both the valence and amount of Cu in magnetite. The valence of Cu in magnetite and the other phases from oxidized granitoids needs to be determined before calculation of oxygen and sulfur fugacity is extracted from the observed Cu levels in the minerals.

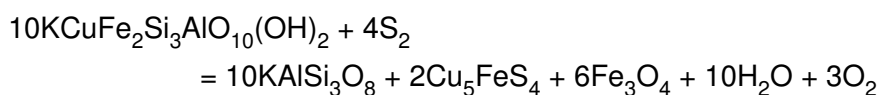
Zinc is buffered in biotite with K-feldspar and sphalerite via the reaction:



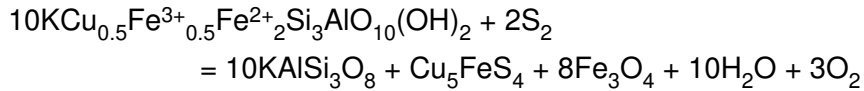
and therefore is buffered by sanidine-sphalerite-fluid. At present this reaction cannot be quantified, although observations of the Zn level in biotite from granitoids for which $f\text{S}_2\text{-}f\text{O}_2\text{-}P(\text{H}_2\text{O})\text{-}T$ have been estimated could be used to derive a fictive value for the ΔG of hendricksonite, depending on the mixing model that was employed as well as the accuracy of $f\text{S}_2\text{-}f\text{O}_2$ and thermobarometry. Copper in biotite is buffered as Cu^{2+} in the presence of bornite-sanidine-fluid by:



and with bornite-magnetite-sanidine-fluid by:



Similar reactions may be balanced with chalcopyrite. However, different reactions buffer Cu^{1+} in biotite with bornite and magnetite:



Application of these and related reactions await careful experiments establishing both the valence and substitution level of Cu in biotite and chlorite. Yet other reactions may be postulated for Zn and Cu in hornblende and also in chlorite if they actually substitute in the structure rather than representing submicroscopic contaminants of metals or sulfides.

Compatible vs. Incompatible Behavior of Cu and Zn

Our results indicate that unaltered silicates have a median value below 10 ppm Cu. Oxide minerals are slightly more enriched in Cu with around 20 ppm as a median value in areas that are not “Cu-rich”. This confirms that Cu is not concentrated in these phases during crystallization because intermediate magmas typically contain 30 to 100 ppm Cu. The low concentration of Cu in these primary magmatic minerals indicates that Cu behaves incompatibly during crystallization of a magma, as long as a sulfide or vapor phase does not form.

The Zn contents of typical mafic silicate and oxide minerals (500 to 1000 ppm) in our study are considerably higher than their Cu contents. This suggests, in turn, that crystallization of most mafic minerals will deplete a melt in Zn. Because the Zn substitutes for Fe, magmas with high Zn/Fe ratios such as granites and aplites are most likely to form a Zn-rich magmatic vapor phase. Zinc partitions strongly into magnetite suggesting that under high $f\text{O}_2$ conditions, when magnetite saturation would occur early, Zn could be stripped from the magma. Therefore, low $f\text{O}_2$ intrusions are probably more likely to generate a magmatic vapor phase that is enriched in Zn.

Zoning patterns in single minerals might be used to gather further information on the proposed incompatible behavior of Cu and compatible behavior of Zn during crystallization. As a simple test of this, we analyzed cores and rims of individual silicate and oxide grains, but these analyses do not show a consistent pattern; rims are not enriched in Cu relative to cores, for instance. A few more complete analytical traverses were made across grains, but most of these were also not definitive. One of the few that with a regular pattern is shown in Figure 7 where the Cu content of a biotite grain from the Keetley volcanic rocks increases toward the edge of the grain, whereas Zn is almost unchanged. The scarcity of systematic zoning in most silicate and oxide grains from the granitoids might reflect their relatively short period of crystallization relative to the interval of time over which the entire magma crystallized.

Post-Crystallization Mobility of Cu

Enrichment of Cu and Zn along altered margins of biotite grains suggests that the rock was permeated by a post-magmatic, Cu- and Zn-bearing vapor phase. Figure 8 shows that these rims can be enriched in Cu or Cu and Zn. The LA-ICP-MS analyses that we have carried out on these rocks show that Cu-rich rims, at least, are widespread in individual samples and

sample suites. They are not a result of anomalous processes related to a single grain. Rather, they appear to have affected the entire rock. If these altered rims record the passage of a magmatic vapor phase, it is likely that they have a systematic distribution within individual intrusions, possibly recording the zones along which deep fluids escaped to shallower levels. This may provide a means of vectoring towards mineralization using samples that do not show significant alteration.

Acknowledgments

This work was funded by BHP-Billiton and by NSF grant EAR-02-30098. Guidance in fieldwork was provided by Patrick Redmond and Ezra Inan of Stanford University, and samples from the Wasatch Range were provided by Thomas Vogel of Michigan State University. Carl Henderson assisted with microprobe analyses.

References Cited

- Al-Hashimi, A.R.K. and Browlow, A.H., 1970, Copper content of biotites from the Boulder Batholith, Montana: *Economic Geology*, v. 65, p.985-992.
- Banks, N. G., 1974, Distribution of Cu in biotite and biotite alteration products in intrusive rocks near two Arizona porphyry copper deposits: *Journal of Research of the United States Geological Survey*, v. 2, p. 195-211.
- Banks, N. G., 1982, Sulfur and copper in magma and rocks: Ray porphyry copper deposit, Pinal County, Arizona, in Titley, S. R., ed., *Advances in Geology of Porphyry Copper Deposits, Southwestern North America*: University of Arizona Press, Tucson, AZ, p. 227-257.
- Blaxland, A.B., 1971, Occurrence of zinc in granitic biotites: *Mineralium Deposita*, v. 6, p. 313-320.
- Brabec, D. and White, W.H., 1971, Distribution of copper and zinc in rocks of the Guichon Creek Batholith, British Columbia: *Canadian Institute of Mining and Metallurgy Special Volume 11*, p 291-297.
- Borrok, D., Kesler, S. E., and Vogel, T. A., 1999, Sulfide mineral in intrusive and volcanic rocks of the Bingham-Park City Belt, Utah: *Economic Geology*, v. 94, p. 1213-1230.
- Burns, R.G., 1993, *Mineralogical Applications Of Crystal Field Theory*, 2nd ed., Cambridge University Press, Cambridge, England. 551 p.
- Chesley, J. T., and Ruiz, J., 1997, Preliminary geochronology on molybdenite mineralization from the Bingham Canyon ore deposit, Utah: *Geological Society of America Abstracts with Programs*, v. 29, p. 282.
- Core, D.P., 2004, Oxygen and sulfur fugacities of granitoids: implications for ore-forming processes: Ph.D. dissertation, University of Michigan, Ann Arbor, MI, 245 p.
- Criss, J. W., 1977, *NRLXRF, A Fortran program for X-ray fluorescence analysis: Users' Reference Manual and General Documentation*, COSMIC DOD-00065.

- Deino, A., and Keith, J. D., 1997, Ages of volcanic and intrusive rocks in the Bingham mining district, Utah: Society of Economic Geologists Guidebook Series, v. 29, p. 91-100.
- Essene, E.J. and Peacor, D.R., 1987, Petedunnite ($\text{CaZnSi}_2\text{O}_6$), a new zinc clinopyroxene from Franklin, New Jersey, and phase equilibria for zincian pyroxenes. *American Mineralogist*, v. 72, p. 157-166.
- Ewart, A., and Griffin, W. L., 1994, Application of proton-microprobe data to trace-element partitioning in volcanic rocks: *Chemical Geology*, v. 117, p. 251-284.
- Fehr, K.T. and Huber, A.L., 2001, Stability and phase relations of $\text{CaZnSi}_3\text{O}_8$, a new phase with feldspar structure in the system CaO-ZnO-SiO_2 : *American Mineralogist*, v. 86, p. 21-28.
- Graybeal, F.T., 1973, Copper, manganese, and zinc in coexisting mafic minerals from Laramide intrusive rocks in Arizona: *Economic Geology*, v. 68, p. 785-798.
- Hendry, D. A., Chivas, A. R., Long, J. V., and Reed, S. J., 1985, Chemical differences between minerals from mineralizing and barren intrusions from some North American porphyry copper deposits: *Contributions to Mineralogy and Petrology*, v. 89, p. 319-329.
- Hendry, D. A. F., Chivas, A. R., Reed, S. J. B., and Long, J. V. P., 1982, Geochemical evidence for magmatic fluids in porphyry copper mineralization. Part II. Ion-probe analysis of Cu contents of mafic minerals, Koloula igneous complex: *Contributions to Mineralogy and Petrology*, v. 78, p. 404-412.
- Holland, H.D., 1959, Stability relations among the oxides, sulfides, sulfates and carbonates of ore and gangue metals: 1. Some applications of thermochemical data to problems of ore deposits: *Economic Geology*, v. 54, p. 184-233.
- Holland, H.D., 1965, Some applications of thermochemical data to problems of ore deposits: 2. Mineral assemblages and the composition of ore forming fluids: *Economic Geology* v. 60, p. 1101-1166.
- Ilton, E. S., and Veblen, D. R., 1988, Copper inclusions in sheet silicates from porphyry Cu deposits: *Nature*, v. 334, p. 516-518.
- Ilton, E. S., and Veblen, D. R., 1993, Origin and mode of copper enrichment in biotite from rocks associated with porphyry copper deposits: a transmission electron microscopy investigation: *Economic Geology*, v. 88, p. 885-900.
- Jiang, S.-Y., Palmer, M.R., Slack, J.F., Yang, J.-H. and Shaw, D.R., 2000, Trace element and rare earth element geochemistry of tourmalinites and related rocks and ores from the Sullivan Deposit and vicinity, southeastern British Columbia: In: *The Geological Environment of the Sullivan Deposit, British Columbia*, Lydon, J.W., Hoy, T., Slack, J.F. and Knapp, M.E., eds, Special Publication 1, Geological Association of Canada, p. 482-495.

- John, D. A., 1989, Geologic setting, depths of emplacement, and regional distribution of fluid inclusions in intrusions of the central Wasatch Mountains, Utah: *Economic Geology*, v. 84, p. 386-409.
- John, D.A., Turrin, B.D. and Miller, R.J., 1997, New K-Ar and $^{40}\text{Ar}/^{39}\text{Ar}$ ages of plutonism, hydrothermal alteration and mineralization in the central Wasatch Mountains, Utah: *SEG Guidebook*, v. 29, p., 47-57.
- Katkov, A.E. and Lykasov, A.A., 2003, Spinel phase relations in the $\text{Fe}_3\text{O}_4\text{-CuFe}_2\text{O}_4$ system: *Inorganic Materials*, v. 39, p. 171-174.
- Kesler S.E., Issigonis, M.J., Brownlow, A.H., Damon, P.E., Moore, W .J., Northcote, K.E. and Preto, V.A., 1975, Geochemistry of biotites from mineralized and barren intrusive systems: *Economic Geology*, 70, p. 559-567.
- Kirkpatrick, P., and Baez, V., 1948, Formation of optical images by X-rays: *Journal of the Optical Society of America*, v. 38, p. 766-774.
- Li, G., Peacor, D.R. and Essene, E.J., 1998, The formation of sulfides during alteration of biotite to chlorite-corrensite: *Clays & Clay Minerals*, v. 46, p. 649-657.
- Lovering, T.G., Cooper, J.R., Drewes, H.D. and Cone, G.C., 1970, Copper in biotite from igneous rocks in southern Arizona as an ore indicator: U. S. Geological Survey Professional Paper, Report: P 0700-B, p. B1-B8,.
- MacDonald, D.J. and Hawthorne, F.C., 1995, Cu-bearing tourmaline from Paraiba, Brazil. *Acta Crystallographica, Section C: Crystal Structure Communications*, v. C51, p. 555-557.
- Parry W.T. and Nackowski, M., 1963, Copper, lead, and zinc in biotites from Basin and Range quartz monzonites.: *Economic Geology*, 58, 1126-1144.
- Parry, W. T., Wilson, P. N., Moser, D., and Heizler, M. T., 2001, U-Pb dating of zircon and $^{40}\text{Ar}/^{39}\text{Ar}$ dating of biotite at Bingham, Utah: *Economic Geology*, v. 96, p. 1671-1683.
- Philippot, P., Menez, B., Drakopoulos, M., Simionovici, A., Snigirev, A. and Snigireva, I., 2001, Mapping trace-metal (Cu,Zn,As) distribution in a single fluid inclusion using a third generation synchrotron light source: *Chemical Geology*, v. 173, p. 151-158.
- Phillips, C.H., Smith, T.W. and Harrison, E.D., 1997, Alteration, metal zoning, and ore controls in the Bingham Canyon porphyry copper deposits, Utah, In: *Geology and Ore Deposits of the Oquirrh and Wasatch Mountains, Utah*, John, D.A. and Ballantyne, G.H., eds., Society of Economic Geologists Guidebook Series v. 29, pp.133-145.
- Redmond, P. B., 2002, Magmatic-hydrothermal fluids and copper-gold ore formation at Bingham Canyon, Utah: Ph.D. thesis, Stanford, University, 228 p.
- Rehrig, W.A. and McKinney, C.N., 1976, The distribution and origin of anomalous copper in biotite: *Mining Engineering*, v. 27, 68 p.

- Rothkopf, A.L. and Fehr, K T., 1998, The chemical potential of hedenbergite in hedenbergite-petedunnite solid solution determined by EMF measurements: *Terra Abstracts*, v. 10, Suppl. 1, p. 53.
- Sapozhnikova, E.Ya., Davidovich, A.G., Roizenblat, E.M., Zinovik, M.A., Kosheleva, L.V., Maslova, V.M. & Markovskii, E.V., 1981, Degree of oxidation of cations in a series of solid solutions of the CuFe_2O_4 - $\text{Cu}_{0.5}\text{Fe}_{2.5}\text{O}_4$ - Fe_3O_4 system: *Zhurnal Neorganicheskoi Khimii*, v. 26, p. 1751-1754.
- Shannon, R.D. (1976) Systematic studies of interatomic distances in oxides, In: *The Physics and Chemistry of Minerals and Rocks*, Strens, R.G.J., ed., John Wiley & Sons, London.
- Smith, J. V., and Rivers, M. L., 1995, Synchrotron X-ray microanalysis, In: Potts, P. J., Bowles, J. F. W., Reed, S. J. B., and Cave, M. R., eds., *Microprobe Techniques in the Earth Sciences*: London, Chapman and Hall, p. 163-233.
- Stimac, J. and Hickmott, D., 1994, Trace-element partition coefficients for ilmenite, orthopyroxene and pyrrhotite in rhyolite determined by micro-PIXE analysis: *Chemical Geology*, v. 117, p. 313-330.
- Vogel, T. A., Cambray, F. W., and Constenius, K. N., 2001, Origin and emplacement of igneous rocks in the central Wasatch Mountains, Utah: *Rocky Mountain Geology*, v. 36, p. 119-162.
- Warnaars, F.W., Smith, W.H., Bray, R.E., Lanier, G. and Shafiqullah, M., 1978, Geochronology of igneous intrusions and porphyry copper mineralization at Bingham, Utah: *Economic Geology* v. 73, p. 1242-1249.
- Willson, W.H., 1979, The distribution of copper in the mafic minerals of the Guichon Creek batholith: M.Sc. thesis, University of Toronto, 182 p.

Figure Captions

- Figure 1. Map of the Bingham-Park City belt showing the location of intermediate volcanic and plutonic rocks. Also shown are the locations of porphyry Cu deposits and Pb-Zn carbonate replacement deposits.
- Figure 2. Histograms showing abundance distributions for Cu and Zn in biotite, pyroxene, hornblende and magnetite from the Bingham-Park City belt. Data are divided into high-Cu (gray) and low-Cu (black) groups as discussed in the text.
- Figure 3. X-ray maps of biotite grain from Clayton Peak stock (CP13-14). A. Fe $K\alpha$ map showing the phases that are present. B. Zn $K\alpha$ map showing that Zn distribution is similar to Fe distribution. C. Cu $K\alpha$ map showing Cu-rich patches in the biotite grain and on the rim of the grain. This map is based on individual analyses at each of the pixels in this image.
- Figure 4. BSE image of boundary of biotite grain in a sample A20-12 from the Alta stock. Edge of the grain has been altered to a mixture of chlorite and sphene. Other grains show thinner alteration rims that also contain magnetite and K-feldspar.
- Figure 5. Cu vs. Zn contents in mafic silicate grains divided into altered and fresh samples on the basis of presence or absence of chloritic alteration in thin section (although the point that was analyzed was free of alteration, alteration was observed in the sample). Analyses for chlorite from Alta are included in part A.
- Figure 6. Cu-Zn, Cu-Fe and Fe-Zn relations for biotite, hornblende, pyroxene, magnetite and feldspar from intrusive igneous rocks of the Bingham-Park City belt. Note that Cu is plotted on a logarithmic axis and Zn and Fe are plotted on arithmetic axes.
- Figure 7. Traverse across biotite from the Keetely volcanic unit showing counts on the Fe, Cu, and Zn $K\alpha$ lines. Zoning shows gradual increase in Cu from core to rim and Zn following Fe with a relatively flat profile. Cu and Zn labels are reversed in this figure.
- Figure 8. Traverses across biotite grains showing counts on the Fe, Cu, and Zn $K\alpha$ lines. A. Biotite and plagioclase from the Alta stock (A20-12). Rims of the biotite grain are enriched in both Cu and Zn and the plagioclase shows patchy zoning of metals. B. Biotite from the Pine Creek stock (PC9-6). Rims of the biotite are enriched in Cu but not Zn. Interior of the grain shows patchy zoning in Cu while Zn follows Fe.

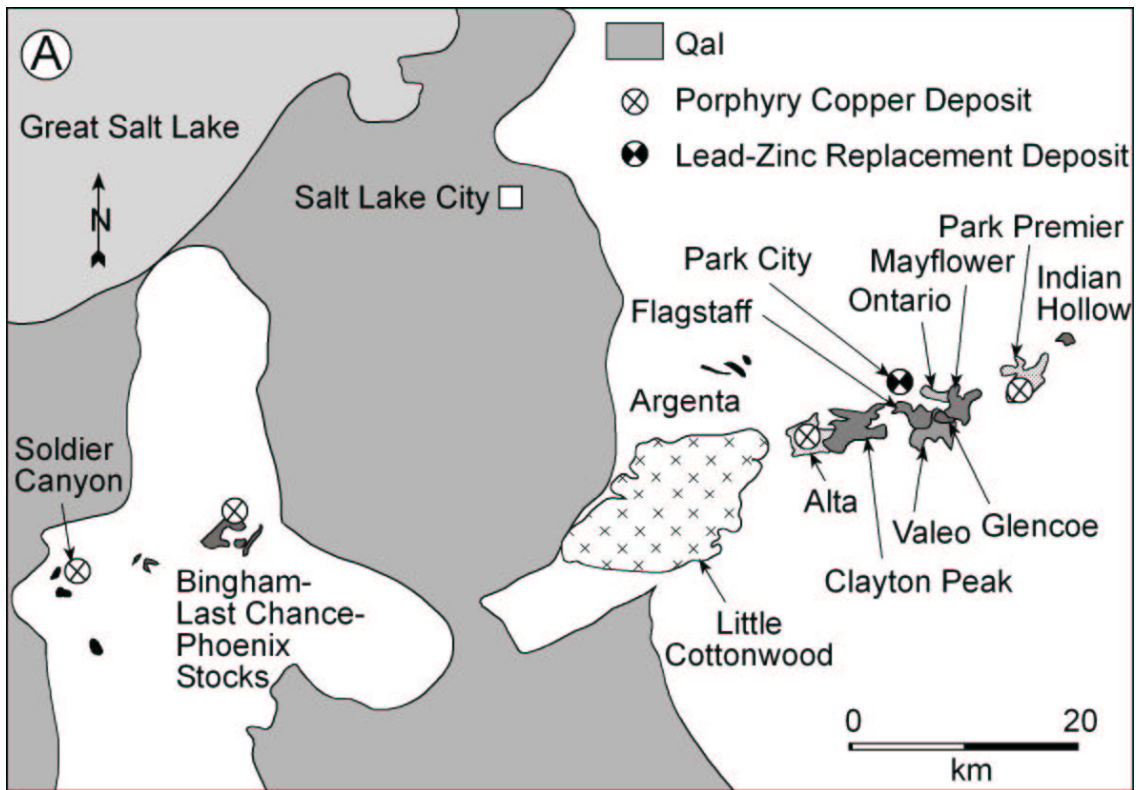


Figure 1

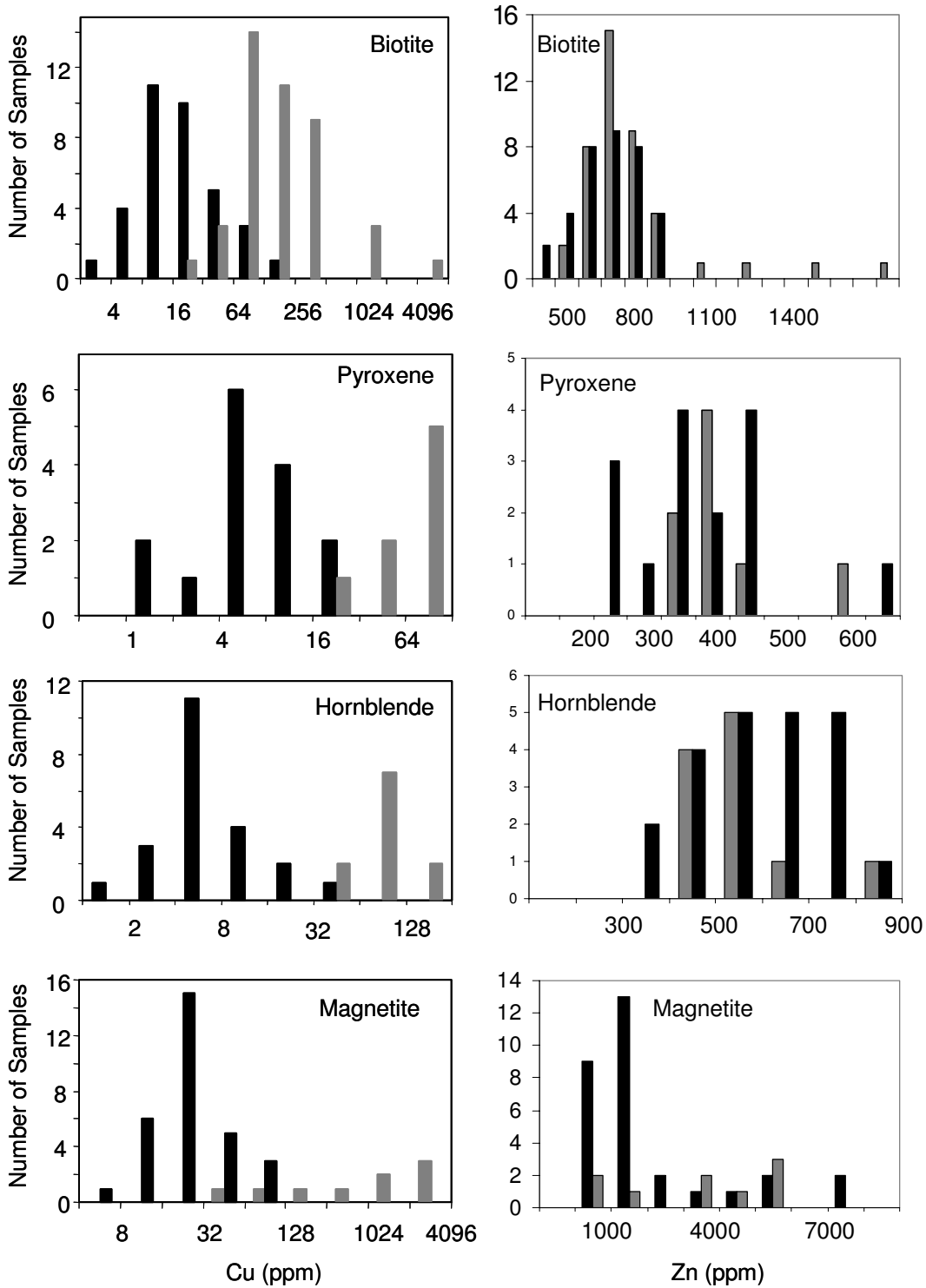


Figure 2

Figure 3

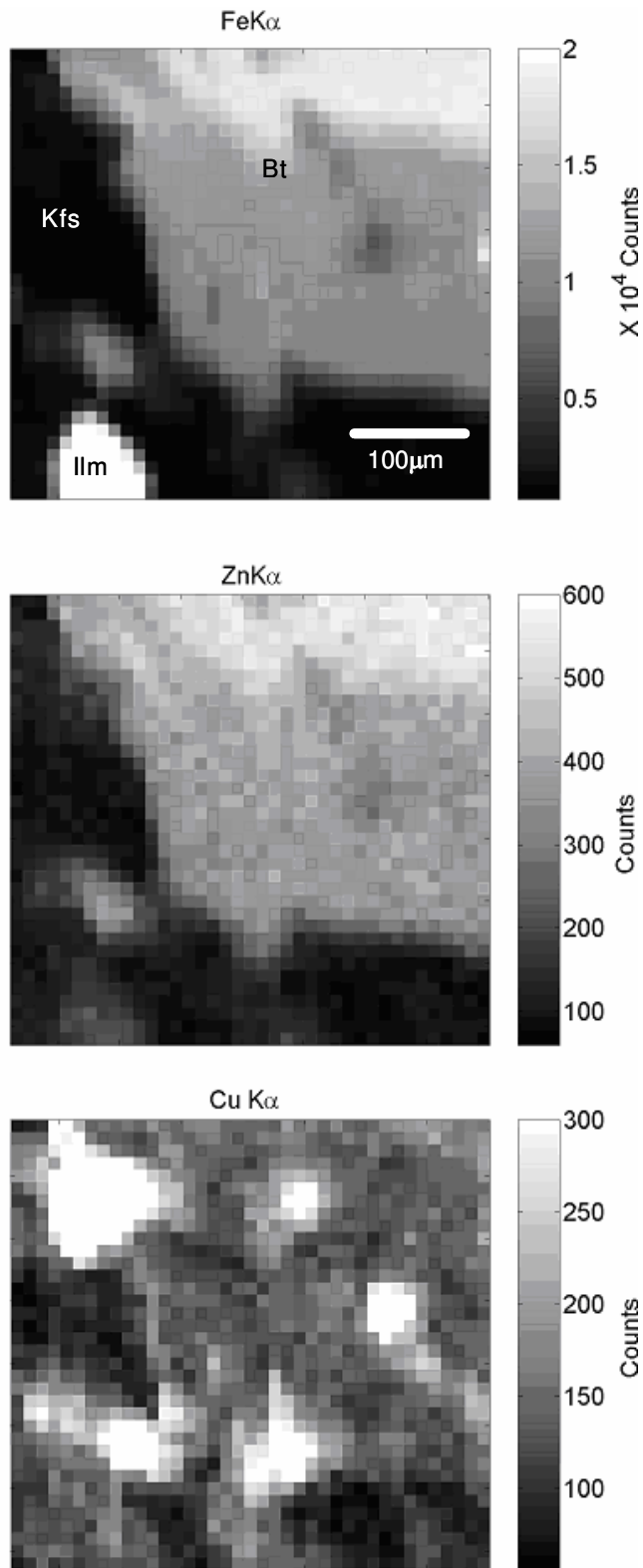


Figure 4

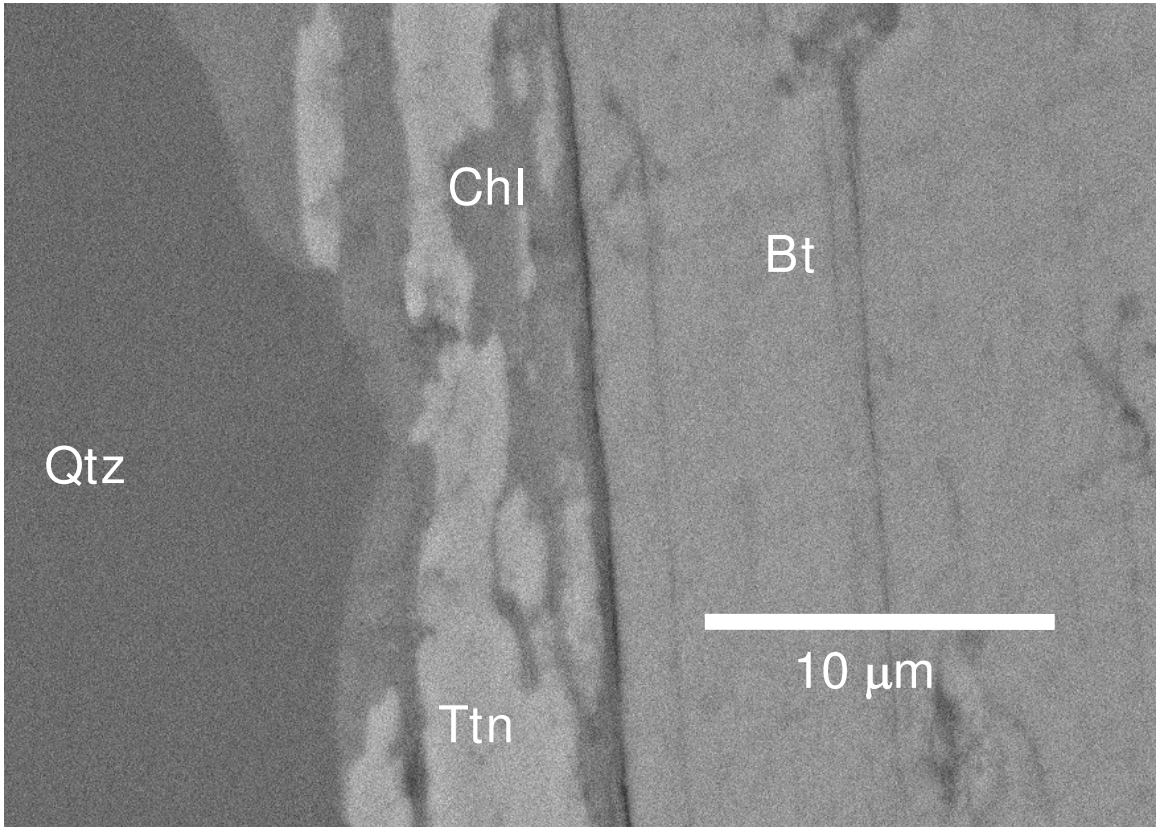


Figure 5

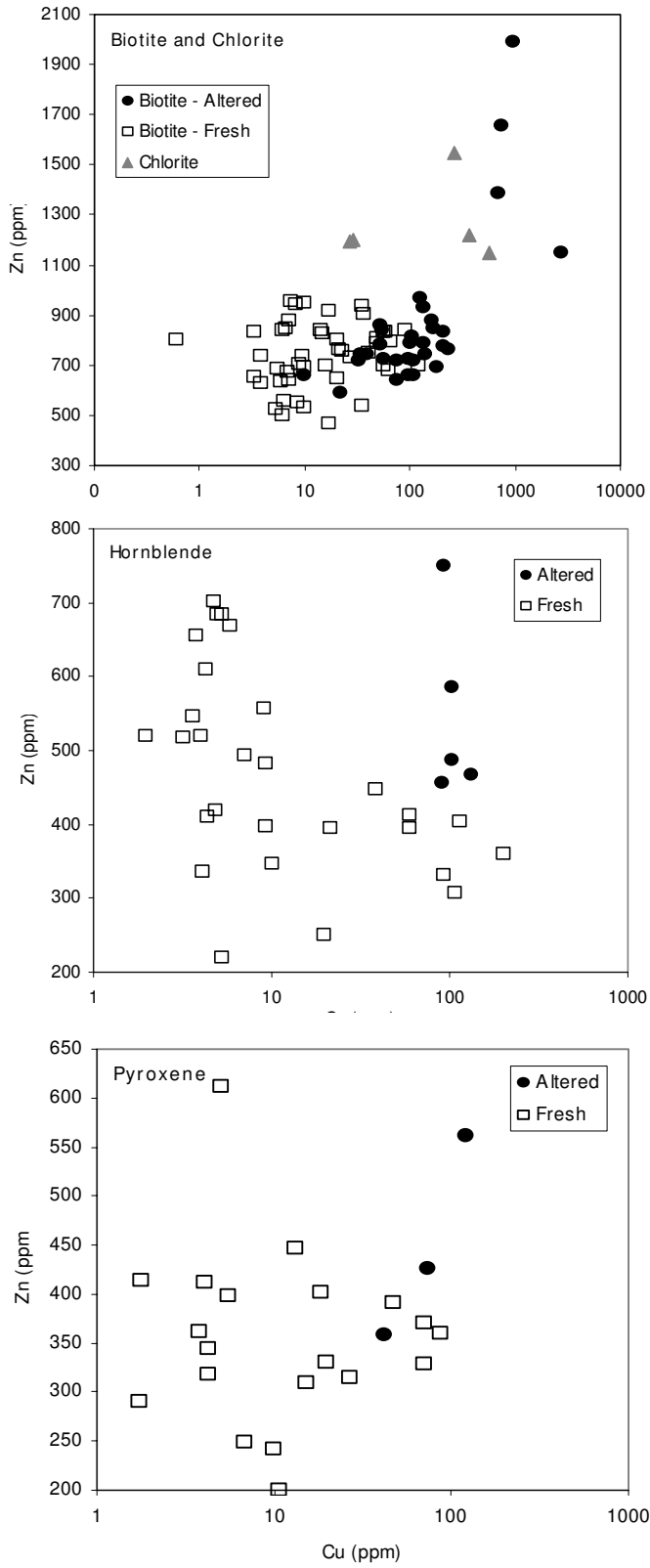


Figure 6

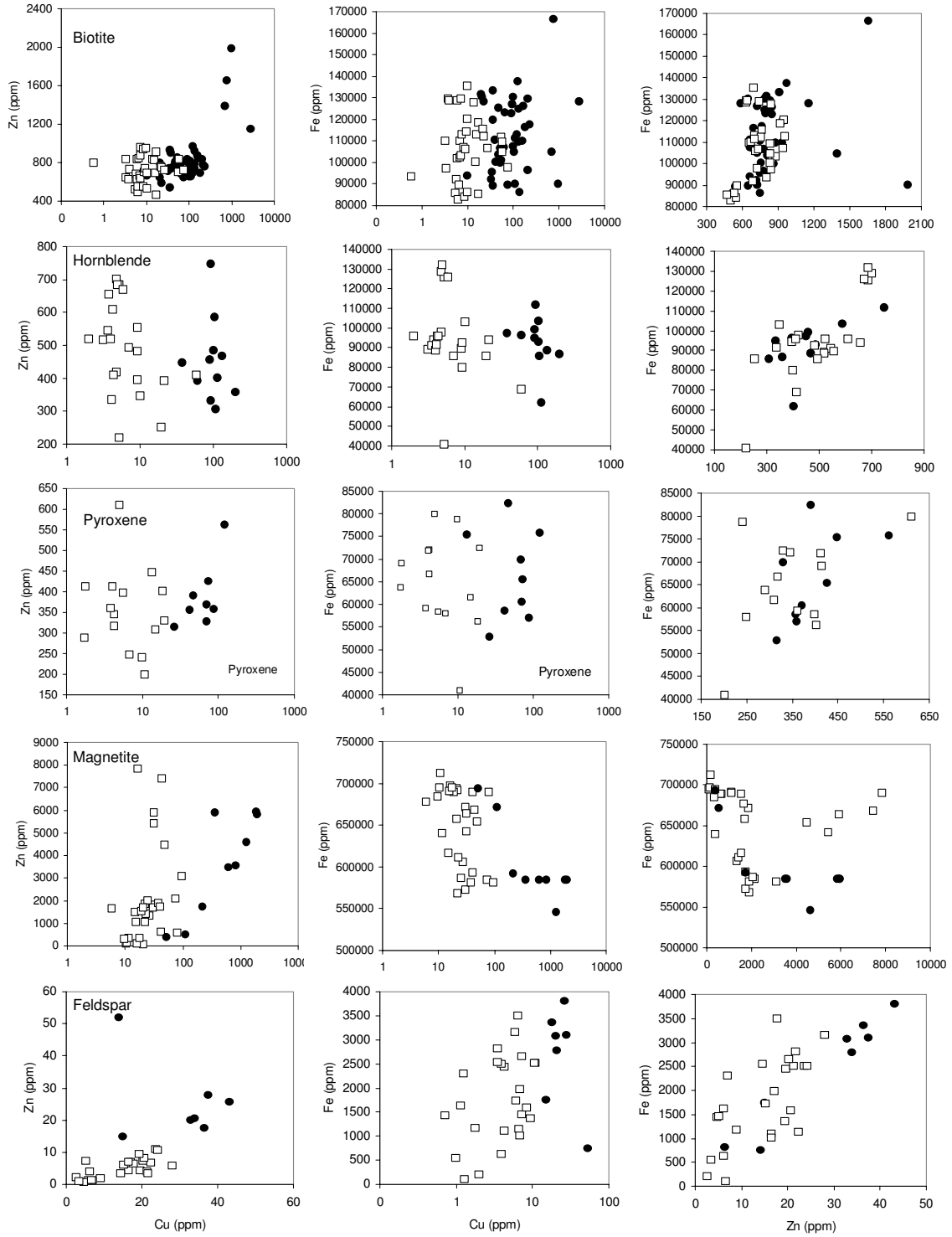


Figure 7

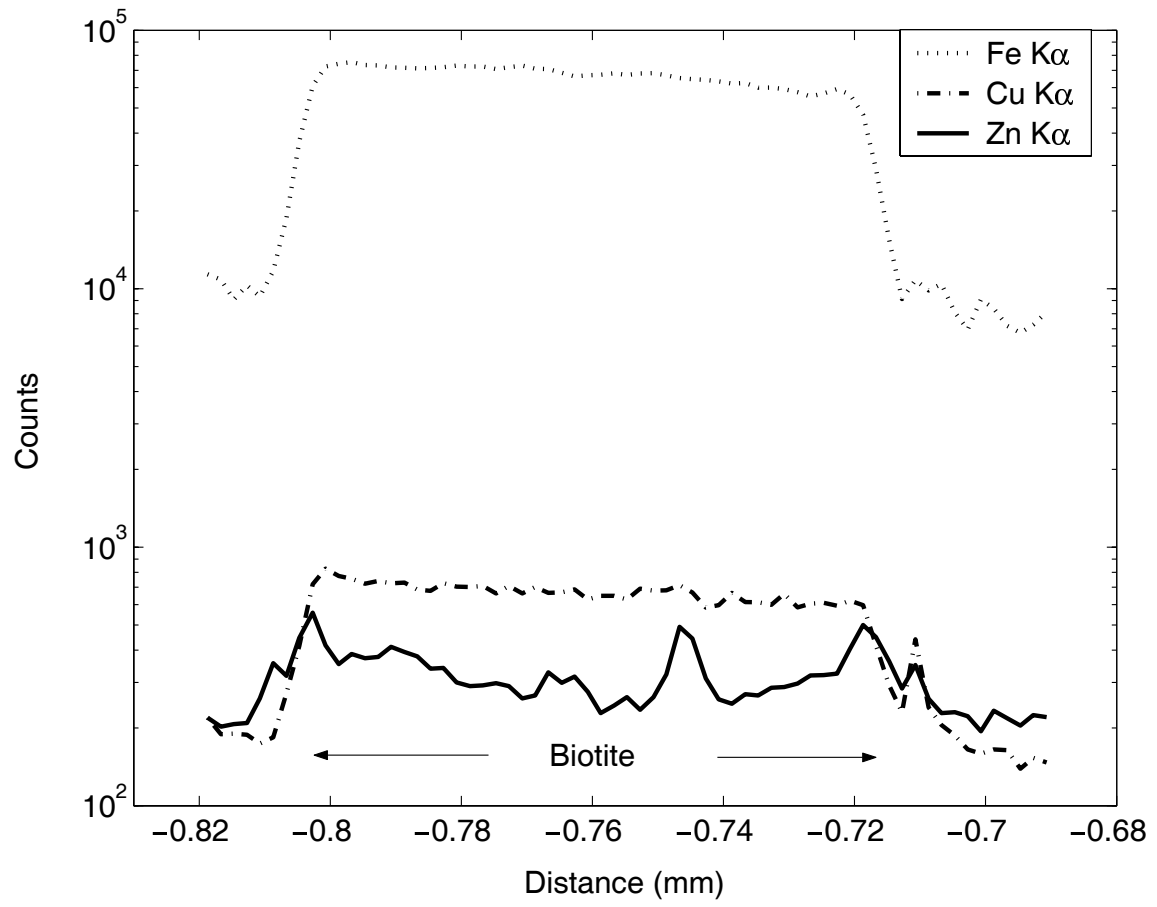


Figure 8

